Substrate and Field Dependence of the SPINOE Transfer to Surface ^{13}C from Hyperpolarized ^{129}Xe

Kevin Knagge, Luis J. Smith,† and Daniel Raftery*

H. C. Brown Laboratory, Department of Chemistry, Purdue University, 560 Oval Drive, West Lafayette, Indiana 47907

Received: August 27, 2004; In Final Form: December 16, 2004

The substrate and field dependencies of surface SPINOE enhancements using optical pumping and magic angle spinning NMR were monitored. Relaxation rates and enhancements were examined to gain an understanding of the parameters that determine the SPINOE enhancement. ^{13}C-labeled deuterated methanol was adsorbed on three different substrates (SnO_2, TiO_2, Ti/SiO_2) with heats of adsorption for xenon ranging from 14.2 to 22.6 kJ/mol. The different heats of adsorption led to a range of xenon coverages and xenon relaxation rates. Using a simple model along with experimental values for the xenon surface polarization and cross- and self-relaxation rates, the ^{13}C signal enhancement could be predicted and compared with experimental enhancement values. Magnetic field dependence studies were also made by monitoring the ^{13}C enhancements via SPINOE from hyperpolarized xenon at fields of 0.075, 4.7, and 9.4 T. The pertinent parameters necessary to achieve maximum SPINOE enhancement are discussed.

Introduction

Many chemical characterization and kinetic studies may be performed with solid-state NMR because of its atomic selectivity and versatility. However, NMR suffers from poor sensitivity primarily because of a low Boltzmann factor at room temperature, and this issue has often been a deterrent to performing NMR surface studies. One method introduced to overcome this problem is spin hyperpolarization via optical pumping.[1−3] Spin exchange between a laser-polarized metal vapor and a noble gas creates a hyperpolarized nuclear spin ensemble. This noble gas ensemble, usually ^3He or ^{129}Xe, can then be transferred to a sample and monitored or used for spin-polarization transfer. Several methods, including spin-polarization induced nuclear Overhauser effect (SPINOE),[4−9] cross-polarization (CP),[10,11] and low-field mixing,[12−14] have been used to transfer polarization from xenon or helium to the nuclei of interest.

The utility and relative inertness of hyperpolarized xenon has created the opportunity for a wide variety of applications, including gas-phase MRI imaging[15−18] as well as NMR studies of high-surface-area substrates and zeolites,[19] blood,[20] and crystallites or crystals.[21−23] With the connection of magic angle spinning to optical pumping experiments,[6,24] a wide variety of surface studies can now be conducted with the advantage of improved spectral resolution. To date, the SPINOE method of polarization transfer has been the most popular and has been examined under many conditions. Transfer characteristics have been examined using liquid xenon,[25] and SPINOE enhancements have been compared to thermal mixing.[14] However, there still remains much to understand about the dynamics of polarization transfer to surface species. In our laboratory, studies have been performed to look at the relaxation dynamics between ^{129}Xe, ^{13}C, and ^1H,[8] and further experiments were performed to examine the effect of temperature on signal enhancement by SPINOE.[26] This variable-temperature study highlighted the fact that xenon surface polarization and surface diffusion could be key components in determining the size of enhancement gained by xenon SPINOE transfer experiments.

In this study, we examine the effect of the substrate on the SPINOE enhancement. We examined surfaces with different xenon heats of adsorption in hopes of gaining an understanding of the effect of Xe coverage and mobility on SPINOE enhancement. ^{13}C NMR of deuterated methanol adsorbed on SnO_2, TiO_2, and $Ti:SiO_2$ surfaces was used to investigate polarization transfer kinetics. We have found that xenon-to-carbon SPINOE behaves differently, depending on the substrate. This behavior is controlled by many factors. The most important factors affecting SPINOE enhancement are the xenon surface polarization, the cross-relaxation rate of polarization transfer, and the relaxation of the ^{13}C target nuclear spin. All three of these factors vary, depending on the surface, xenon coverage, flow rate, initial xenon polarization, and a variety of other factors. We also examined the field dependence of SPINOE. In the past, the field dependence of the signal-to-noise of hyperpolarized xenon has been examined.[27] In this study, we examined the field dependence of polarization transfer of hyperpolarized xenon to ^{13}C in $^{13}CD_3OD$ on a silica substrate.

Theory. The steady-state NOE enhancement gained from the dipolar interaction between two nuclear spin ensembles has been well characterized and can be described by the following expression:[28]

$$\eta_I = \sigma_{IS}/\rho_I \tag{1}$$

where η_I is the polarization enhancement (given by $(I(t) - I_0)/I_0$) gained by nucleus I, σ_{IS} is the cross-relaxation rate of polarization from nucleus S to nucleus I, and ρ_I is the self-relaxation rate of nucleus I. The cross relaxation is driven by the dipolar interaction and, therefore, propagates through space without requiring any chemical bonding. The two important rates in this reaction can also be defined mathematically. The self-

* Author to whom correspondence should be addressed. E-mail: raftery@purdue.edu.

† Present address: Clark University, Worcester, MA 01610.

10.1021/jp046113c CCC: $30.25
Published on Web 02/15/2005

relaxation rate is given by:

$$\rho_I = \gamma^2 B_{loc}{}^2 J(\omega_I) \propto \tau_C/(1 + \tau_C{}^2 \omega_I{}^2) \quad (2)$$

where τ_C is the correlation time, ω_I is the Larmor frequency of nucleus I, and $J(\omega_I)$ is the spectral density. The other important quantity is the cross-relaxation rate, which may be defined using:[29]

$$\sigma_{IS} = \frac{\hbar^2 \cdot \gamma_I^2 \cdot \gamma_S^2}{10 \cdot r_{IS}^6}\left(\frac{6\tau_c}{1 + (\omega_I + \omega_S)^2 \cdot \tau_C^2} - \frac{\tau_C}{1 + (\omega_I - \omega_S)^2 \cdot \tau_C^2}\right) \quad (3)$$

where γ_I and γ_S are the gyromagnetic ratios of spin I and S, respectively, r_{IS} is the distance between spins I and S, and ω_I and ω_S are the Larmor frequencies of spins I and S, respectively. This equation may be solved with a polynomial function to determine the correlation time. However, if the spin system is assumed to be in the extreme narrowing limit ($(\omega\tau_c)^2 \ll 1$), the simplified expression:[3]

$$\sigma_{IS} = \frac{\hbar^2 \cdot \gamma_I^2 \cdot \gamma_S^2}{10 r_{IS}^6} \cdot 5\tau_C \quad (4)$$

may be used to obtain the correlation time.

The interaction of hyperpolarized ^{129}Xe with a deuterated ^{13}C-labeled methoxy species chemisorbed on a surface can be characterized by a simple two-spin model system. We have shown that the polarization of this system may be defined using modified Solomon equations.[26,30] These equations may be solved under the assumption that the hyperpolarized xenon polarization delivered to the sample does not change significantly with time. This assumption will lead to the steady-state approximation for xenon surface polarization discussed in Smith et al.[26] given by:

$$\eta_{Xe}^{SS} \approx \frac{\eta_{Xe}^{OP} \cdot \rho_{Xe}^{OP}}{\rho_{Xe}^{eff}} \quad (5)$$

where ρ_{Xe}^{OP} is the rate xenon flows into and out of the sample rotor, η_{Xe}^{OP} is the polarization enhancement of gas-phase xenon, and ρ_{Xe}^{eff} is the effective surface-relaxation rate. ρ_{Xe}^{eff} is not exactly the same as the xenon T_1 at the surface since hyperpolarized xenon leaves the sample rotor during the course of the experiment, introducing another component to the apparent relaxation of xenon besides the normal spin−lattice relaxation. The steady-state solution for the surface carbon enhancement may then be given by:

$$\eta_C^{SS} = \frac{\gamma_{Xe}}{\gamma_C}(\eta_{Xe}^{SS}) \frac{\sigma_{CXe} \cdot \rho_{Xe}}{\rho_C \cdot \rho_{Xe} - \theta(\sigma_{CXe}^2)} \quad (6)$$

where γ_{Xe} and γ_{Xe} are gyromagnetic ratios and θ is the surface xenon coverage. In the case of SPINOE experiments, eq 6 may be simplified to:

$$\eta_C^{SS} = \eta_{Xe}^{SS} \cdot \frac{\sigma_{CXe}}{\rho_C} \cdot \frac{\gamma_{Xe}}{\gamma_C} \quad (7)$$

because $\sigma_{CXe} \ll 1$. Once the cross-relaxation rate between the two spins has been determined, the correlation time of the interaction between these two spins may be solved for using eq 4. It was observed from experimentation that measurements could be considered in the extreme narrowing limit for the correlation time ($\tau_C \cdot \omega_I \ll 1$) at low fields, but the validity of this approximation is somewhat questionable at higher fields (400 MHz).

Experimental Section

All surface-dependent experiments were conducted using a home-built optical pumping apparatus coupled to a 200-MHz NMR spectrometer. Field-dependent experiments were determined using the same apparatus except at 400 MHz, where a Chemagnetics instrument and 5-mm rotor were used. The optical pumping apparatus consisted of a glass cell containing a few grams of rubidium metal. The cell was placed in an oven that was heated to 423 K, providing the optimum amount of rubidium in the gas phase for optical pumping. The oven was surrounded by a set of Helmholtz coils, placing the cell in a 20-G field. A 25-W fiber-coupled diode laser (Optopower) centered at 795 nm was used as the laser source. The laser was brought through a light circular polarizer and onto the glass cell. The beam radius and the radius of the cell were both approximately 2.5 cm. A previously mixed combination of 2% Xe (26% ^{129}Xe), 2% nitrogen, and 96% helium was flowed through the cell at a rate of 160 mL/min. The cell pressure was maintained at approximately 4 atm. The gas mixture was then carried through 3 m of Teflon tubing onto the sample contained within a 7-mm rotor inside the 200-MHz NMR. The rotor was spun at 3.5 kHz using nitrogen gas. All samples were cooled to temperatures between 130 and 190 K by precooling the bearing gas in a liquid nitrogen bath.

BET experiments were performed by placing a few hundred milligrams of sample into a specifically developed test tube designed to limit headspace above the sample. The sample was placed on a gas manifold and cooled to between 153 and 213 K using a variety of temperature baths (chloroform/nitrogen, toluene/nitrogen, acetone/dry ice, acetone/nitrogen, ethanol/nitrogen). Incremented pressures of xenon were then exposed to the sample, allowing 5 min for adsorption and equilibration to take place before the pressure was incremented. Xenon coverage and heats of adsorption can be derived using BET isotherm theory.[31] The heat of adsorption has a weak linear dependence on temperature over a small temperature range, making it possible to interpolate coverage values for temperature values unreachable through experimentation.

All samples were prepared on a gas manifold. SiO_2 (Cab-o-sil, M-5, Cabot Corporation) was prepared by heating at 413 K under vacuum for 10 h. TiO_2 (Degussa) and SnO_2 (Nanotek) were prepared by dehydrating under vacuum for 10 h at 773 K. The samples were then exposed to 760 Torr of oxygen for 10 h. Ti/silica was prepared by dehydrating silica (Cab-o-sil, HS-5) under vacuum for 10 h at 773 K. The silica was then exposed to $TiCl_4$ (Aldrich) in a quantity sufficient to provide a monolayer coverage in a sealed test tube for 24 h. The sample was then placed in 25 mL of distilled water and allowed to set for 4 h. Finally, the sample was run through vacuum filtration and placed in a vacuum oven for approximately 6 h. $^{13}CD_3OD$ (Cambridge Isotopes) was chemisorbed onto certain surfaces by freezing 1.5 monolayers of methanol onto each sample, sealing the test tube, and heating at 513 K for 10 h. The samples were then exposed briefly to vacuum to eliminate all physisorbed methanol, leaving only chemisorbed methanol. Samples were stored and loaded into the sample rotors in a drybox to avoid air and water contamination.

Field-dependent experiments were performed by obtaining ^{13}C NMR enhancements and T_1 relaxation rates at 143 K with the sample spinning at 4 kHz. The relaxation rate for the low-

TABLE 1: S/N Ratios of ^{13}C Signals from SPINOE Experiments of $^{13}CD_3OD$ on Silica[a]

	(S/N)/mg sample/ transient	
field, T (MHz)	with HP ^{129}Xe	without HP ^{129}Xe
0.075 (3.2)	0.31	N/A
4.7 (200)	0.19	0.050
9.4 (400)	0.94	0.45

[a] S/N ratios are divided by the amount of sample (mg) and $\sqrt{n}$, where n is the number of transients taken to obtain the signal.

field experiments could not be determined experimentally, so it was approximated by using eq 2 and assuming the correlation time was constant over all fields. Experiments at 200 and 400 MHz were performed by allowing the xenon gas mixture to flow onto the sample while it was spinning. Data were then taken using pulse-acquire experiments with a recycle delay of 30 s. The low-field experiments were performed by placing the probe underneath the magnet. The field was approximately 750 G at the probe−coil region. The sample was cooled and spun at the same speed as in the high-field experiments. The xenon mixture was allowed to flow onto the sample for 30 s, the probe was then swiftly lifted into the magnet, and a single-shot spectrum was acquired. No signal was seen without the benefit derived from hyperpolarized xenon.

All surface-dependent experiments were performed at 200 MHz. Cross-relaxation rates were determined by saturating the carbon signal, waiting some incremented time for xenon-to-carbon polarization transfer, and then recording the carbon signal. The intensities were then fitted to an exponential build-up curve with the following functional form:

$$I(t) = I_0\left[-\left(\frac{\sigma_{CXe}}{\rho_C}\cdot\frac{\gamma_{Xe}}{\gamma_C}\cdot\eta_{Xe}+1\right)e^{-\rho_C t}+\frac{\sigma_{CXe}}{\rho_C}\cdot\frac{\gamma_{Xe}}{\gamma_C}\cdot\eta_{Xe}\right]+I_0 \quad (8)$$

and the cross-relaxation rates were then determined.

Results and Discussion

Field Dependence. The S/N of ^{13}C signals at different fields may be seen in Table 1. All S/N values were divided by the amount of sample and $\sqrt{n}$, where n is the number of transients. This was done to standardize all data. It should be noted that the S/N of the data taken at 400 MHz is approximately 9 times higher because of the combined effects of a larger magnetic field and a better (commercial) spectrometer. From Table 1, it may be seen that the S/N of the sample that interacted with xenon at low field was greater than that of the sample that interacted with xenon at 200 MHz. Because data was taken under the same conditions, it is most likely that this increase is due to increased SPINOE enhancement. Actual SPINOE enhancements may be calculated by dividing the S/N with hyperpolarized xenon after n transients by the S/N without hyperpolarized xenon after the same n transients. This calculation is performed for both the 200 and the 400 MHz data, and the values of 2.8 and 1.1 were obtained, respectively. Again, this shows that the SPINOE enhancement increases with a decrease in field strength, in agreement with previous studies by Cherubini, et al.[14] This phenomenon is believed to arise because of an increase in cross relaxation with a decrease in field that results from a decrease in energy splittings between spin states, making the transfer of spin polarization more efficient.

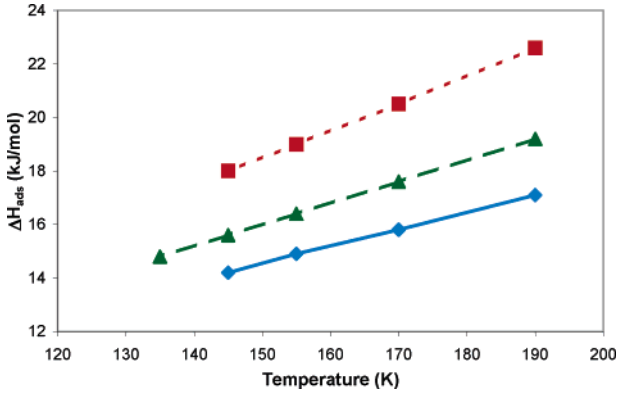

Figure 1. Heats of adsorption vs temperature for each of the samples at different experimental temperatures. Heats of adsorption were calculated from BET data. (◆) Methoxy species on SnO_2, (▲) methoxy species on TiO_2, (■) methoxy species on Ti:SiO_2.

Substrate Dependence. BET studies were performed on different surfaces using xenon to obtain the heat of adsorption of xenon on these surfaces. Heats of adsorption for the three different samples at a variety of different temperatures may be seen in Figure 1. The heat of adsorption has a small but linear dependence on temperature over the experimental temperature range, which allowed for interpolation of heat of adsorption values. BET data were then used to obtain the xenon coverages at a variety of temperatures.

A plot of the ^{13}C signal enhancement (η_C) versus temperature may be seen in Figure 2a. For two of the samples, SnO_2 and Ti:SiO_2, the enhancements reach maximum values at a given temperature. This behavior was seen previously in Smith et al.[26] The maximum enhancement achieved and the temperature at which it is achieved both differ strongly, depending on the substrate. As can be seen in Figure 2a, methoxy species adsorbed on the TiO_2 surface and the Ti:SiO_2 surface show a much larger enhancement than methoxy species adsorbed on the SnO_2 surface. Also, the maximum enhancement is achieved at approximately 170 K for both the Ti:SiO_2 surface and the SnO_2 surface, while the maximum enhancement is not seen for the TiO_2 surface, occurring out of the range of measurements we performed in this study. (At warm temperatures, the enhancement must go to zero as the xenon surface coverage becomes negligible.) These measurements indicate just how dependent SPINOE enhancement is on the substrate used.

Figure 2b shows the enhancement of the carbon signal achieved from SPINOE on different surfaces versus the xenon coverage on each surface. Each sample tends to display similar behavior. As the coverage was increased, a maximum enhancement was achieved at a certain coverage, and then enhancement decreased. This behavior may be due to xenon staying on the surface too long at cold temperatures such that it fills the available surface sites, restricting freshly polarized xenon from reaching the adsorbed methoxy species. When the temperature was decreased below 130 K, the enhancement decreased to zero as xenon ice formed on the surface (seen in the ^{129}Xe NMR spectra for these samples). It is believed that the xenon ice completely blocks the surface from freshly polarized xenon and, therefore, enhancement is only achieved for a short period until this frozen xenon relaxes.

Another major factor that affects carbon enhancement from the SPINOE effect using hyperpolarized xenon is the xenon surface relaxation rate. Carbon enhancement versus xenon relaxation may be seen in Figure 2c. The enhancements are low at short xenon T_1's because xenon is relaxing before it can effectively transfer its polarization to the methoxy species on

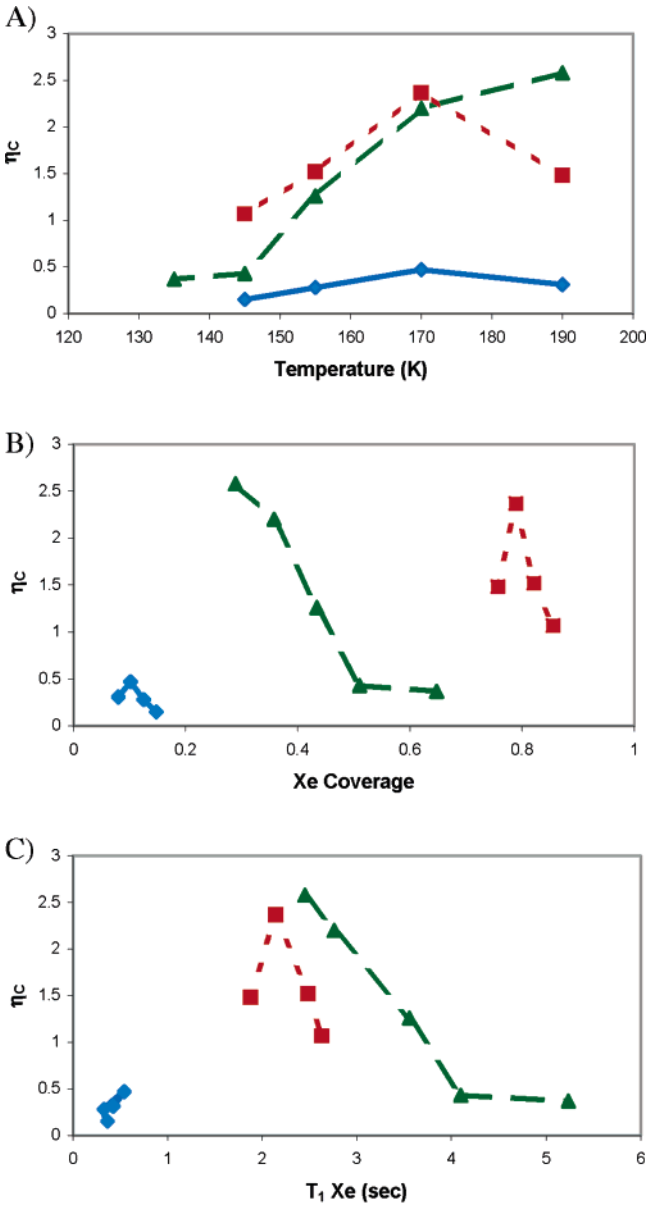

Figure 2. ^{13}C enhancement gained by $^{13}CD_3OD$ adsorbed on different oxide surfaces from SPINOE experiments vs (A) sample temperatures, (B) Xe coverage on each sample, and (C) the Xe T_1 on the surface. (◆) Methoxy species on SnO_2, (▲) methoxy species on TiO_2, (■) methoxy species on Ti:SiO_2 for all figures.

the surface. Here, xenon is most likely relaxing quickly because of interactions with surface atoms of the substrate (such as chemical shift anisotropy modulation, dipolar coupling, or possibly paramagnetic impurities at or near the surface); therefore, the Xe surface polarization (η_{SS}^{Xe}) is relatively low. Enhancement rises until the T_1 of xenon is approximately 2.5 s. At this point, xenon relaxation becomes dependent on xenon exiting the rotor as well as normal spin-relaxation processes. The apparent xenon T_1 no longer increases at colder temperatures as it approaches a maximum value entirely dependent on the rate of xenon exiting the rotor.

The relationship of cross-relaxation rate, carbon relaxation rate, and xenon surface polarization to overall enhancement may be seen in eq 7 and in Figure 3. The figure shows the measured enhancement gained versus the solution to eq 7 using individually determined experimental values for η_{Xe}^{SS}, ρ_C, and σ_{CXe}. Data from a previous study (Smith et al.)[26] were also added for comparison. That study examined adsorbed $^{13}CH_3OH$ on SiO_2,

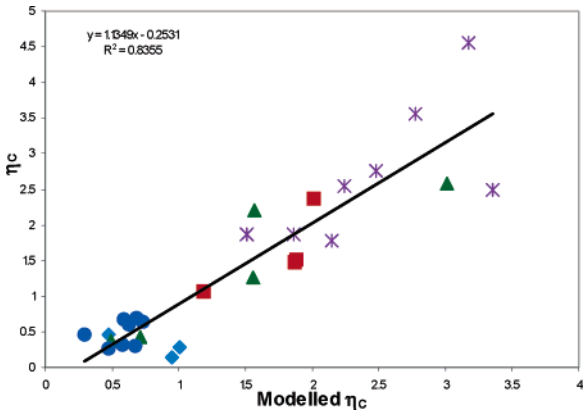

Figure 3. ^{13}C enhancement gained by $^{13}CD_3OD$ adsorbed on different oxide surfaces from SPINOE experiment vs the modeled enhancement (eq **7**) with the best fit line included. (◆) Methoxy species on SnO_2, (▲) methoxy species on TiO_2, (■) methoxy species on Ti:SiO_2, (●) and methoxy species on SiO_2 (*) from a previous study on SiO_2.[26]

and thus the measured ^{13}C enhancements result from $^{129}Xe-^{13}C$ SPINOE plus $^{1}H-^{13}C$ NOE or $^{129}Xe-^{13}C$ SPINOE minus $^{1}H-^{13}C$ NOE. The modeled data were derived following methods described in Smith et al.[26] Although there is considerable scatter about the best-fit line, the observed enhancement appears to obey eq 7 as a reasonable approximation to eq 6. The observed enhancements are slightly greater than the expected values (represented by the slope of the best-fit line being approximately 1.1).

Some of the different variables involved in SPINOE enhancement were also fitted to gain an understanding of their dependence on experimental conditions. The cross-relaxation rate is considered to behave according to the Arrhenius expression:[26]

$$\sigma_{IS} = \frac{\hbar^2 \cdot \gamma_I^2 \cdot \gamma_S^2}{10 r_{IS}^6} 5\tau_0 \exp(-E_A/RT) \qquad (9)$$

because of the temperature dependence of the correlation time. Figure 4a shows the relationship between temperature and cross-relaxation rate (^{13}C enhancement data were added from a previous study by Smith et al.[26] for comparison). In Figure 4a, the cross-relaxation rate was scaled by coverage to give a rate constant that is not dependent on the amount of xenon on the surface. Additional data on the cross relaxation as a function of temperature (Figure 1S) and xenon coverage (Figure 2S) are available as Supporting Information. It may be seen in Figure 4a that cross-relaxation rates decrease with decreasing temperature, following the Arrhenius expression given in eq 9, with the possible exception of the SnO_2 data. The rates are relatively level for the SnO_2 and SiO_2 samples and may fall somewhat at higher temperatures, possibly as a result of the coverage being too low to obtain a large amount of polarization transfer. The fit of cross-relaxation data gives values for the activation energy E_A and the correlation time constant τ_0, and the values may be seen in Table 2. It should be noted that eq 9 may only be used by assuming we are in the extreme narrowing limit for the correlation time. We believe this is a good assumption because correlation times obtained using both eqs 3 and 4 were the same to four significant figures. It may be seen that activation energies for the carbon/xenon interaction are far less than surface adsorption energies of xenon seen in Figure 1. This leads us to believe that the activation energy most likely corresponds to a weaker lateral diffusional motion rather than an adsorption of

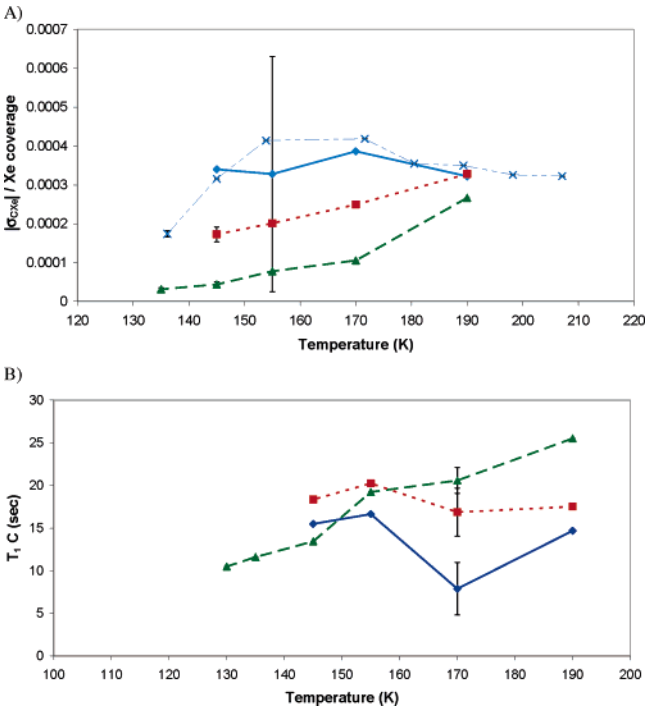

Figure 4. (A) The absolute value of the xenon-to-carbon cross-relaxation rates (s^{-1}) and (B) carbon T_1 vs temperature. (◆) Methoxy species on SnO_2, (▲) methoxy species on TiO_2, (■)methoxy species on Ti:SiO_2, (×) methoxy species on SiO_2.[26] Representative error bars are included. Errors for the SnO_2 sample are large in (A) because of the low values of the cross relaxation and the low coverage.

TABLE 2: Parameters Characterizing Cross-Relaxation Rate Constant σ_{CXe} by Fitting Experimentally Determined Values to an Arrhenius Behavior Using Eq 9[a]

substrate	τ_0, s	E_A, J/mol
SnO_2	8.01×10^{-11}	900
TiO_2	6.44×10^{-9}	6300
Ti:SiO_2	1.51×10^{-9}	2000

[a] The distance between nuclei was chosen to be 3.7 Å according to previous work by Smith et al. (ref 26).

gas-phase xenon (adsorption energy). Also, the correlation time is on the scale of 10^{-9}−10^{-11} s, while the xenon sticking time is more in the range of 10^{-6} s. This implies that the correlation time and the interaction of xenon with carbon surface spins is likely associated with a diffusional motion or "hopping" on the surface rather than an actual phase change of xenon adsorbing to and desorbing from the surface. It may also be seen in Table 2 that the correlation time for ^{13}C/^{129}Xe interaction on SnO_2 is much shorter than the other samples. This is leads to smaller cross-relaxation rates σ_{CXe}, one of the causes of smaller η_C enhancement seen in Figure 2.

Figure 4b shows the relationship between the carbon T_1's and temperature. Equation 7 demonstrates the importance of the carbon T_1 to the overall enhancement. Essentially, if the carbon T_1 is too small, any polarization gained through hyperpolarized xenon would quickly relax before any sizable build up of the enhancement could be obtained. Figure 4b shows that the carbon T_1's are relatively constant over the temperature range, and only one data point drops below 10 s.

The product of xenon surface polarization and xenon coverage was also examined in an effort to describe the enhancement trends. Figure 5 shows that this product is linear for SnO_2 and TiO_2 samples (fitted lines added for visual clarity), where the slope is a combination of the temperature dependence factors

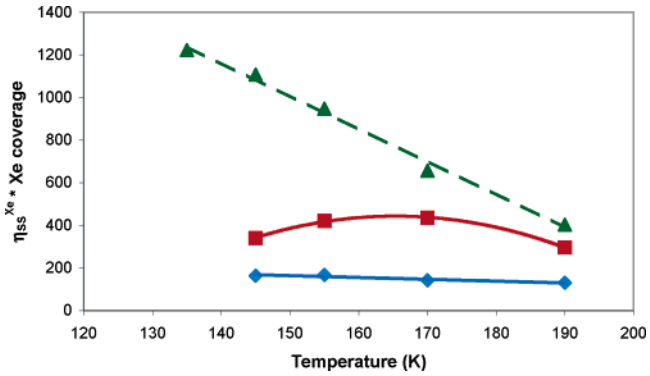

Figure 5. Steady-state Xe polarization multiplied by Xe coverage vs temperature. (◆) Methoxy species on SnO_2, (▲) methoxy species on TiO_2, (■) methoxy species on Ti:SiO_2. Linear and parabolic fits were added for visual clarity.

of coverage and the xenon T_1. However, the Ti:SiO_2 sample appears to behave more parabolically (fitted curve added for visual clarity). One possibility for this behavior is that the xenon coverage is approaching one full monolayer. As the coverage exceeds a monolayer, xenon becomes trapped on the surface and is not replenished, leading to complete xenon relaxation of adsorbed xenon atoms and the value η_{Xe}^{SS} approaching zero. This behavior is possibly occurring on the Ti:SiO_2 at 80−85% xenon coverage. The product of coverage and xenon surface polarization should asymptotically approach zero as the temperature decreases in all samples. It should also asymptotically approach zero in all samples as the coverage approaches zero, but this behavior was not studied here. It should also be noted that, depending on the nature of the monolayer formed, the Ti:SiO_2 sample may have multiple sites, introducing a new, not yet interpreted level of complexity.

One might expect that the surface signal enhancement would be proportional to the number of polarized xenon nuclei on the surface (estimated by the product of coverage and xenon surface polarization). However, the behavior seen in these studies does not necessarily reflect the expected relationship. Because of the complex behavior of xenon surface polarization near monolayer coverage (especially on the Ti:SiO_2 sample), it is currently difficult to model the relationship of xenon surface polarization to temperature on the basis of information inputs such as the xenon surface T_1, xenon flow rate, and xenon coverage. This, in turn, makes the modeling of SPINOE enhancement η_C of CD_3OD species on the surface quite challenging at this stage. More studies of this type on a broader range of materials is needed to make further progress in modeling the SPINOE polarization transfer.

Conclusions

The use of hyperpolarized xenon in optical-pumping NMR experiments has been shown to increase the sensitivity of NMR. SPINOE experiments are becoming more common as a method of polarization transfer to surface species from hyperpolarized xenon. However, this polarization transfer is not completely understood and has yet to be fully optimized. Substrate properties, such as heat of adsorption, coverage, and xenon relaxation rate on the surface as well as the strength of the magnetic field seem to be key variables in determining the SPINOE enhancement obtained. Heat of adsorption affects the xenon coverage and the sticking time on the surface. Hyperpolarized xenon coverage plays a key role in the SPINOE enhancement, with degree of enhancement increasing as coverage is increased up to a certain point, dependent on the surface.

It may also be seen that two major relaxation rates dominate the enhancement gained, the xenon surface relaxation rate, and the cross-relaxation rate of transfer between xenon and carbon. The carbon T_1 at the surface is important when it is very short, although this was not the case for the samples examined. The xenon surface relaxation rate in part determines the xenon surface polarization at steady state along with the coverage and xenon replenishment (flow) rate and initial gas-phase xenon polarization. The cross-relaxation rate determines how efficiently this surface polarization is used. The cross relaxation appears to increase as the field decreases. However, field cycling experiments are necessary to completely verify this, and the complex experimental design complicates this approach. It was also found that the xenon surface and cross-relaxation rates are both dependent on surface conditions such as the substrate and experimental temperatures. SPINOE enhancement is in turn strongly affected by both of these rates. With measurements on a broader range of systems, we hope to develop a more predictive model for surface-species enhancement via hyperpolarized xenon and SPINOE.

Acknowledgment. We thank Jay Smith, Ernesto MacNamara, and Charles Rice for their help in assembly of the optical-pumping setup and spectrometer. This work was funded by NSF (CHE01-09626) and donors of the Petroleum Research Fund, administered by the American Chemical Society.

Supporting Information Available: Additional information. This material is available free of charge via the Internet at http://pubs.acs.org.

References and Notes

(1) Raftery, D.; Long, H.; Meersmann, T.; Grandinetti, P. J.; Reven, L.; Pines, A. *Phys. Rev. Lett.* **1991**, *66*, 584−587.
(2) Walker, T. G.; Happer, W. *Rev. Mod. Phys*. **1997**, *69*, 629−642.
(3) Goodson, B. M. *J. Magn. Reson*. **2002**, *155*, 157−216.
(4) Navon, G.; Song, Y.-Q.; Room, T.; Appelt, S.; Taylor, R. E.; Pines, A. *Science* **1996**, *271*, 1848−1851.
(5) Room, T.; Appelt, S.; Seydoux, R.; Hahn, E. L.; Pines, A. *Phys. Rev. B* **1997**, *55*, 11604−11610.
(6) Raftery, D.; MacNamara, E.; Fisher, G.; Rice, C. V.; Smith, J. *J. Am. Chem Soc*. **1997**, *119*, 8746−8747.
(7) Pietrass, T.; Seydoux, R.; Pines, A. *J. Magn. Reson*. **1998**, *133*, 299−303.
(8) MacNamara, E.; Rice, C. V.; Smith, J.; Smith, L. J.; Raftery, D. *Chem. Phys. Lett*. **2000**, *317*, 165−173.
(9) Song, Y.-Q. *Concepts Magn. Reson*. **2000**, *12*, 6−20.
(10) Long, H. W.; Gaede, H. C.; Shore, J.; Reven, L.; Bowers, C. R.; Kritzenberger, J.; Pietrass, T.; Pines, A.; Tang, P.; Reimer, J. *J. Am. Chem. Soc*. **1993**, *115*, 8491−8492.
(11) Smith, J.; Smith, L. J.; Knagge, K.; MacNamara, E.; Raftery, D. *J. Am. Chem. Soc*. **2001**, *123*, 2927−2928.
(12) Bowers, C. R.; Long, H. W.; Pietrass, T.; Gaede, H. C.; Pines, A. *Chem. Phys. Lett*. **1993**, *205*, 168−170.
(13) Appelt, S.; Haesing, F. W.; Baer-Lang, S.; Shah, N. J.; Blumich, B. *Chem. Phys. Lett*. **2001**, *348*, 263−269.
(14) Cherubini, A.; Payne, G. S.; Leach, M. O.; Bifone, A. *Chem. Phys. Lett*. **2003**, *371*, 640−644.
(15) Albert, M. S.; Cates, G. D.; Driehuys, B.; Happer, W.; Saam, B.; Springer, C. S.; Wishnia, A. *Nature* **1994**, *370*, 199.
(16) Song, Y.-Q.; Goodson, B. M.; Pines, A. *Spectroscopy* **1999**, *14*, 26.
(17) Cherubini, A.; Bifone, A. *Prog. Nucl. Magn. Reson. Spectrosc*. **2003**, *42*, 1.
(18) Choquet, P.; Hyacinthe, J. N.; Duhamel, G.; Grillon, E.; Leviel, J. L.; Constantinesco, A.; Ziegler, A. *Magn. Reson. Med*. **2003**, *49*, 1014−1018.
(19) Nossov, A.; Haddad, E.; Guenneau, F.; Gedeon, A. *Phys. Chem. Chem. Phys*. **2003**, *5*, 4473−4478.
(20) Bifone, A.; Song, Y.-Q.; Seydoux, R.; Taylor, R. E.; Goodson, B. M.; Pietrass, T.; Budinger, T. F.; Navon, G.; Pines, A. *Proc. Natl. Acad. Sci. USA* **1996**, *93*, 12932−12936.
(21) Terskikh, V. V.; Moudrakovski, I. L.; Du, H.; Ratcliffe, C. I.; Ripmeester, J. A. *J. Am. Chem. Soc*. **2001**, *123*, 10399−10400.
(22) Stahl, D.; Mannstadt, W.; Gerhard, P.; Koch, M.; Jansch, H. J. *J. Magn. Reson*. **2002**, *159*, 1−12.
(23) Jansch, H. J.; Gerhard, P.; Koch, M.; Stahl, D. *Chem. Phys. Lett*. **2003**, *372*, 325−330.
(24) Brunner, E.; Haake, M.; Pines, A.; Reimer, J. A.; Seydoux, R. *Chem. Phys. Lett*. **1998**, *290*, 112−116.
(25) Fitzgerald, R. J.; Sauer, K. L.; Happer, W. *Chem. Phys. Lett*. **1998**, *284*, 87−92.
(26) Smith, L. J.; Smith, J.; MacNamara, E.; Knagge, K.; Raftery, D. *J. Phys. Chem. B* **2001**, *105*, 1412−1421.
(27) Cross, A. R.; McDonald, M.; Parra Robles, J.; Santyr, G. E. *J. Magn. Reson*. **2003**, *162*, 241−249.
(28) Derome, A. E. *Modern NMR Techniques for Chemistry Research*; Pergamon: Oxford, 1987.
(29) Slichter, C. P. *Principles of Magnetic Resonance*; Springer-Verlag: Berlin, 1990.
(30) Solomon, I. *Phys. Rev*. **1955**, *99*, 559−565.
(31) Flood, E. A. *The Solid−Gas Interface*; Marcel Dekker: New York, 1967.